The Atomistic Structure of Yttria Stabilised Zirconia at 6.7mol%: an *ab initio* Study

Michael A. Parkes[a,b], *David A. Tompsett*[b], *Mayeul d'Avezac*[d], *Gregory J.Offer*[e], *Nigel P. Brandon*[a] *and Nicholas M. Harrison*[b]

[a]Department of Earth Science and Engineering, Imperial College London, SW7 2BP, UK

[b]Department of Chemistry, Imperial College London, London, SW7 2AZ, UK

[d]Research Software Development Team, Research Computing and Facilitating Services, University College London, London WC1E 6BT, UK

[e]Department of Mechanical Engineering, Imperial College London, SW7 2AZ, UK

Keywords: solid oxide fuel cell, yttria stabilised zirconia, *ab initio*, density functional theory, empirical potential, Born-Mayer-Huggins, ReaxFF, point charge model.

Abstract

Yttria stabilized zirconia (YSZ) is an important oxide ion conductor used in solid oxide fuel cells, oxygen sensing devices, and for oxygen separation. Doping pure zirconia (ZrO_2) with yttria (Y_2O_3) stabilizes the cubic structure against phonon induced distortions and this facilitates high oxide ion conductivity. The local atomic structure of the dopant is, however, not fully understood. X-ray and neutron diffraction experiments have established that, for dopant concentrations below 40mol% Y_2O_3, no long range order is established. A variety of local structures have been suggested on the basis of theoretical and computational models of dopant energetics. These studies have been restricted by the difficulty of establishing force field models with predictive accuracy or exploring the large space of dopant configurations with first principles theory. In the current study a comprehensive search for all symmetry independent configurations (2857 candidates) is performed for 6.7mol% YSZ modelled in a 2x2x2 periodic supercell using gradient corrected density functional theory. The lowest energy dopant structures are found to have oxygen vacancy pairs preferentially aligned along the ⟨2 1 0⟩ crystallographic direction in contrast to previous results which have suggested that orientation along the ⟨1 1 1⟩ orientation is favourable. Analysis of the defect structures suggests that the Y^{3+} - O_{vac} interatomic separation is an important parameter for determining the relative configurational energies.

Current force field models are found to be poor predictors of the lowest energy structures. It is suggested that the energies from a simple point charge model evaluated at unrelaxed geometries

is actually a better *descriptor* of the energy ordering of dopant structures. Using these observations a pragmatic procedure for identifying low energy structures in more complicated material models is suggested. Calculation of the oxygen vacancy migration activation energies within the lowest energy ⟨2 1 0⟩ oriented structures gives results consistent with experimental observations.

Introduction

Yttria stabilised zirconia (YSZ) is an oxide ion conductor at elevated temperatures. The $(Y_2O_3)_{0.1}(ZrO_2)$ composition, commonly referred to as 10mol% Y_2O_3, has an ionic conductivity of $0.03 Scm^{-1}$ at $1273K$[2]. In addition to the material's favourable anionic conductivity, YSZ has several other properties that make it an appropriate electrolyte material for solid oxide fuel cells (SOFCs). These include its low electrical resistivity, mechanical stability, and chemical stability towards other SOFC materials, including lanthanum manganese oxide ($LaMnO_3$), lanthanum strontium cobalt ferrite (LSCF), and nickel[3].

At a typical SOFC anode, YSZ forms an interface with a catalytic metal and a gas phase, which is known as the triple phase boundary (TPB). There is a growing interest in developing a physical and chemical understanding of YSZ and its surfaces as a basis for detailed models of the chemical reactions occurring at the TPB which govern the performance of the fuel cell and, of particular current interest, its degradation with use[4–10]. In addition, understanding the mechanism by which oxygen ions conduct through the YSZ structure is of great interest for the development of improved oxide ion conductors[11]. A detailed knowledge these processes is currently inhibited

by a poor understanding of the local distribution of dopant Y^{3+} ions and oxygen vacancies (O_{vacs}) in the bulk crystal, and at its surfaces and interfaces[12].

Zirconia (ZrO_2) exhibits three crystal structures under standard pressure[13]. At room temperature it adopts a monoclinic (m) structure which undergoes phase transitions to tetragonal (t) and cubic (c) structures at 1443K and 2643K respectively. The cubic phase exhibits the highest oxide ion (O^{2-}) conductivity making it the most technologically useful. Doping zirconia with Y_2O_3 is used to stabilise the cubic phase and reduce the temperature at which the tetragonal to cubic phase transition occurs. Typical doping concentrations include 3, 8, 10 and 12mol%. The exact Y_2O_3 concentration that stabilises YSZ in the cubic phase is uncertain[14]; X-ray diffraction data suggests that 8mol% is the minimum concentration at which the cubic phase is stable at room temperature[15–17]. For doping concentrations above 40mol%, the ordered compound $Zr_3Y_4O_{12}$ is formed[18–20].

The low temperature instability of the cubic phase of ZrO_2 is indicated in density functional theory (DFT) calculations at the athermal limit which find imaginary phonon frequencies at and near the X-point of the first Brillouin zone[21–23]. Based on calculations of the phonon spectrum using the generalised gradient approximation (GGA) to DFT a frequency of the imaginary mode at X has been reported to be $i217cm^{-1}$ [24]. The eigenvector of this mode involves displacements of oxygen anions along the ⟨1 0 0⟩ direction breaking the cubic symmetry which, upon full relaxation of the cell and internal coordinates, results in a barrier free transformation of the cubic structure to the observed low temperature tetragonal phase[25].

Doping zirconia with Y_2O_3 is isoelectronic; for each formula unit two Y^{3+} ions, which have effective negative charges relative to the lattice ions, replace two Zr^{4+} ions and charge neutrality is maintained by the formation of an oxygen ion vacancy (O_{vacs}), which has an effective charge of plus two relative to the lattice ions. In Kröger-Vink notation this substitution is;

$$Y_2O_3 \xrightarrow{ZrO_2} 2Y'_{Zr} + V_o^{\cdot\cdot} + 3O_o^X$$

The O_{vac} facilitates the conduction of O^{2-} ions through the lattice, with the ionic conductivity depending on the Y_2O_3 concentration. For low concentrations the conductivity rises rapidly with the number of dopants, and reaches a maximum at 8mol%[26,27]. At higher concentrations the conductivity falls gradually and it has been suggested that that inter-dopant interactions inhibit O-ion transport due to the increased electrostatic interaction between dopant cations and vacancies[2,3]. A detailed model of the pathways and interactions involved has proved elusive in the absence of reliable atomistic models of the dopant geometries.

The local atomistic structure and distribution of the dopants in YSZ has been the topic of much theoretical and experimental research. From X-ray and neutron diffraction data it has been argued that the dopant structure is highly disordered with multiple, distinct dopant clusters formed[27]. The low contrast in the X-ray and neutron scattering powers of Zr^{4+} and Y^{3+} ions has made it extremely difficult to deduce the relative positions of the Y^{3+} and O_{vac} species, or to determine the local geometry of the dopant structures[18]. On the basis of X-ray absorption fine structure spectroscopy (EXAFS)[28–30], solid state ^{89}Y-MAS-NMR experiments[31], DFT total energy calculations[32], and a thermodynamic models based on cluster expansions[33], it has been

established that, in general, Y^{3+} ions prefer 8-fold O-coordination while the Zr^{4+} ion O-coordination is reduced to 7-fold from the 8-fold coordination of ZrO_2. These results are consistent with the so called "next nearest neighbour" (NNN) model of the dopant structure, where the O_{vac} is found in the first O-coordination sphere of Zr^{4+} and the second O-coordination sphere of Y^{3+}. The preference for NNN type defect structures is in contrast to the nearest neighbour (NN) model of the defect structure, proposed on the basis of early neutron diffraction, EXAFS, and a simple point charge model of the ionic interactions[34–37], in which Y^{3+} ions have 7-fold O-coordination, with the O_{vac} in the first O-coordination shell of Y^{3+}. In recent work we established that for the isolated dopant (3.2mol%) DFT calculations strongly support the stability of NNN structures with NN structures at least 0.25 eV per formula unit higher in energy. For this reason, in what follows we exclude NN structures from those considered as candidates for the lowest energy configurations in YSZ[24].

There are many possible defect topologies that are consistent with the preference for Zr^{4+} to have 7-fold and Y^{3+} to have 8-fold O-coordination. At dopant concentrations above 3.2mol% there are many thousands of possible configurations that fulfil this constraint[24]. Given the combinatorial complexity of the system, the development of a methodology that facilitates the prediction of low energy NNN defect topologies, without the need for computationally demanding first principles calculations, is of significant interest[24]. In recent work the GGA-DFT energies of a complete set of symmetry inequivalent isolated defects computed at the dilute limit (3.2mol% Y_2O_3) with unrelaxed, and fully relaxed internal atomic coordinates, were compared to a variety of structural and computationally undemanding *descriptors* in an attempt to identify useful correlations. In particular, the electrostatic energy of a simple point charge model, calculated at

the unrelaxed geometries of the defects, a strain relaxation energy computed within the harmonic approximation, and the total energy of the relaxed structures predicted by the best available Born-Mayer-Huggins (BMH) polarisable shell model. NN structures were neglected as the GGA-DFT always predicts these structures to be significantly energetically unfavourable compared to NNN and longer range structures. The conclusions of that study was that for the NNN, and indeed of all long-range NNNN and NNNNN type structures, the simple point charge model is found to be a good predictor of the likely low energy GGA-DFT structures. In contrast, the strain relaxation energy computed within the harmonic approximation was a poor descriptor of the stability of long-range NNN or greater structures, but a good descriptor of the high energy short-range NN type structures. The BMH polarisable shell model correlated poorly with the energetic trends predicted by GGA-DFT[24].

At the dilute limit of 3.2mol%, the Y_2O_3 dopant clusters are isolated and the inter-cluster interactions are negligible. At the more technologically relevant 6.7mol% concentration, dopant clusters interact, and the formation energy of the doped system increases by ~ 0.2 eV[24]. A key feature is the interaction between the $O_{vacs,}$ which, in a formal charge electrostatic model, have effective charges of +2e relative to the lattice ions. O_{vacs} would be expected to repel one-another and to maximise their separation. Nevertheless, diffuse neutron scattering data has established that O_{vacs} preferentially associate in pairs. It also suggests that the O_{vac} pairs are oriented along the crystallographic ⟨1 1 1⟩ direction at dopant concentrations between 10 and 24mol%, without forming a long range ordered phase[18,26,27]. Theoretical support for the short range ordering of dopant induced vacancies in ⟨1 1 1⟩ directions has also been provided by previous DFT total energy calculations of models representing 17mol% and 40 mol%[19,20]. More recent DFT

calculations of models representing 6.7mol% and 10.4mol%[38,39] also suggest that dopant induced vacancies preferentially associate in pairs along ⟨1 1 1⟩. Ostanin *et al.*[39] studied several representative structures of 6.7mol%, 10.4mol% and 14.3mol% YSZ where the O_{vacs} were located in the second O-coordination sphere of the Y^{3+} ions and the first O-coordination sphere of the Zr^{4+} ions confirming the strong preference for Y^{3+} to have 8-fold O-coordination. It is notable that in this study alignment of the vacancy pair along the ⟨1 0 0⟩, ⟨1 1 0⟩, ⟨1 1 1⟩, ⟨2 1 1⟩, and ⟨2 2 2⟩ directions were considered, while the possible alignment along ⟨2 0 0⟩, ⟨2 1 0⟩, ⟨2 2 0⟩, and ⟨2 2 1⟩ was neglected. In the fluorite crystal structure of c-ZrO_2, there exist two symmetry independent configurations in which O_{vac} pairs can align along the ⟨1 1 1⟩ direction, one of which gives rise to a 6 fold O-coordinated Zr^{4+} ion, and the other gives rise to two 7 fold O-coordinated Zr^{4+} ions. Although distinct these configurations have the same interatomic separation of the vacancies. Based on GGA-DFT total energies of chemically motivated structures, Ostanin *et al.* also concluded that the configuration with two 7 fold O-coordinated Zr^{4+} ions is the most stable[39]. The electron paramagnetic resonance (EPR) spectrum of YSZ for dopant concentrations below 12mol% contains a prominent trigonal (T centre) peak in samples where vacancies have been introduced by chemical reduction or exposure to ionizing radiation[40–43]. This peak has been interpreted as a vacancy-vacancy pair lying in a ⟨1 1 1⟩ direction neighbouring a Ti^{3+} impurity[44–46].

While the evidence outlined above suggests that oxygen vacancy pairs align along the ⟨1 1 1⟩ direction this conclusion has been obtained in the absence of a comprehensive search of all configurations for a structural model at 6.7mol% YSZ. In the current work the GGA-DFT total energies of a complete set of 6.7mol% YSZ substitutions in a 96 ion 2x2x2 supercell of c-ZrO_2

are computed. The cell is chosen to allow maximum separation of the dopant ions and vacancies for its volume (up to ~10 Å). Subject to the constraint of maintaining 8-fold O-coordination of Y^{3+} ions this results in 2857 symmetry inequivalent configurations. For each structure the internal coordinates have been fully relaxed. We use the energies and geometries of the resulting structures to reanalyse the distribution of O_{vac} pairs within the system and thus all possible orientations of the vacancy pair are considered: ⟨1 0 0⟩, ⟨1 1 0⟩, ⟨1 1 1⟩, ⟨2 0 0⟩, ⟨2 1 0⟩, ⟨2 1 1⟩, ⟨2 2 1⟩, and ⟨2 2 2⟩. In contrast to previous studies the ⟨2 1 0⟩ orientation of the vacancy pair is found to be significantly lower in energy than any other orientation. Geometric analysis of the dopant clusters is used to identify features of the defects such as; Y^{3+} - O_{vac} interatomic separation, and Y^{3+} - Y^{3+} interatomic separation, that correlate to the relative DFT energies.

The large database of structures and energies generated also allows us to reassess and quantify the accuracy of previous findings for 3.2mol% YSZ. We use the database to assess the efficacy of Coulomb based point charge and the currently best available interatomic potential models (both Born-Meyer-Huggins and the more recent ReaxFF parameterisation) for describing the relative energies of dopant configurations. From this we propose a pragmatic method for identifying low energy dopant configurations in more complicated morphologies such as surfaces interfaces and nanostructures.

Computational Details

DFT plane-wave calculations, detailed below, were performed alongside empirical force field calculations based on the Born-Mayer-Huggins (BMH) form and the reactive force field (ReaxFF) form, as implemented in the GULP code[47].

A periodic model of 6.7mol% YSZ is created by introducing two Y_2O_3 units into a 96 atom 2x2x2 supercell of the conventional crystallographic c-ZrO_2 cell. There are 4,530,960 possible defect topologies when four substitutional Y^{3+} ions and two O_{vacs} are introduced into the ideal fluorite sites of the 2x2x2 c-ZrO_2 supercell. Taking into account all translational and space-group symmetries this can be reduced to 8985 symmetrically inequivalent structures[48], of which 2857 structures are long-range NNN, NNNN, and NNNNN type structures where the O_{vacs} reside in the first O-coordination sphere of Zr^{4+}, and the second or greater O-coordination sphere of Y^{3+}. We distinguish between "*unrelaxed"* structures, where all ions and vacancies reside on the ideal fluorite sites of c-ZrO_2, and *"relaxed"* structures where the internal coordinates of the periodic unit cell have been optimised.

DFT calculations were performed using the projector augmented wave (PAW) method as implemented in the VASP code[49]. The effects of electronic exchange and correlation are approximated using the Perdew-Burke-Ernzerhof[50] (PBE) GGA exchange-correlation (XC) functional was used for all calculations. In order to render the calculation of a large number of configurations computation tractable we make use of the softer oxygen PAW potential distributed with VASP and thus a plane-wave energy cutoff of 283 eV. The PAW potentials were generated using the following electronic configurations $2s^2$, $2p^4$ for oxygen, $4s^2$, $4p^6$, $4d^2$, $5s^1$ for yttrium and $4s^2$, $4p^6$, $4d^3$, $5s^1$ for zirconium and further details may be found in *Kresse and*

Joubert[51]. In tests on 33 randomly selected configurations calculations with this potential reproduced, to within 25 meV per supercell, the energy differences obtained from calculations with harder oxygen PAW potential and a plane-wave energy cutoff of 400 eV[1,49]. All defect structure calculations were performed at the computed zero-pressure DFT lattice constant of c-ZrO_2 (a = 10.23). Relaxation of the lattice parameters would potentially introduce effects of long range order, which experimentally is known to not be present. The defect structure, rather, is disordered and retains the cubic symmetry. As will be discussed, the low energy defect structure that we obtain stabilizes the cubic structure, consistent with experimental observation. A 3×3×3 Monkhorst-Pack[52] grid was used for Brillouin zone sampling. All internal degrees of freedom were optimised using a quasi-Newton algorithm without symmetry constraints, until all atomic forces were less than 0.01eV/$Å^{-1}$. Consistent with the formal valence in the defect structure, our test calculations find that spin polarization collapses to zero in all cases. Therefore, the results of non-spin polarized calculations are presented throughout this work.

The BMH polarisable shell model based on formal ionic charges has been used previously to model defects in zirconia[13,38,53–55]. The form of the potential and the parameters are presented in *equation 1* and *Tables 1 & 2*. The Zr-O interaction parameters were determined by Dwivedi and Cormack[56] by fitting to the experimental lattice and dielectric constants of t-ZrO_2. Those for Y-O and O-O were determined by Lewis and Catlow[57]. In addition to t-ZrO_2, the Zr-O potentials have been shown to accurately reproduce the experimental lattice constants of stabilised c-ZrO_2, but not those of m-ZrO_2, which is found to be unstable with respect to an orthorhombic phase. The Y-O potential accurately reproduces the experimental lattice constants of bixbyite Y_2O_3[13].

$$\varphi_r = \frac{q_a q_b}{r} + Aexp^{(-r/\rho)} - \frac{B}{r^6} \qquad \textit{-equation 1}$$

Where, r is the interionic distance between species with charges q_a and q_b.

Table 1: YSZ Born-Mayer-Huggins potential parameters.

Short Range Interactions				
Interaction	A / eV	ρ / Å	B / eVÅ^6	Cut off / Å
$Zr^{4+}....O^{2-}$	985.87	0.3760	0.0	10
$O^{2-}....O^{2-}$	22764.00	0.1490	27.88	12
$Y^{3+}....O^{2-}$	1345.10	0.3491	0.0	10

Table 2: Polarisable shell model parameters for the Born-Mayer-Huggins potential.

Shell Model		
Species	γ / e	k / eVÅ^{-2}
O^{2-}	-2.077	27.290
Zr^{4+}	1.35	169.617

A bond order potential, in the ReaxFF form, was developed by A. van Duin & W. Goddard III recently to facilitate molecular dynamics simulations of the SOFC TPB[9,10,58,59] by fitting to the following database computed using DFT: Mulliken charge populations of bixbyite Y_2O_3, c-ZrO_2, and $BaZr_{0.75}Y_{0.25}OH_{0.25}$, the equation of states of for several Y metal, Zr metal, and YZr alloy phases, the equations of states for several theoretical and experimentally observed phases of ZrO_2 and Y_2O_3, the equation of states of $Y_2Zr_6O_{15}$ (14.3mol% YSZ), and the relative energies of six 7.1mol% YSZ defect structures. The parameters defining the ReaxFF potential can be found in the most recent publications of A van Duin *et al*. [9,10]

In what follows we assess correlations between data sets using a simple regression analysis. Correlations are described by the coefficient of determination (R^2), which is the square of the Pearson correlation coefficient. The coefficient of determination has a value between 0 and 1 where 0 is no correlation and 1 is a perfect correlation.

Results

Low Energy Crystal Structure of 6.7mol% YSZ from DFT

Initially we investigate how the total energy of the defects changes with the crystallographic orientation of the O_{vac} pair. The 2857 symmetry inequivalent structures were sub-divided into categories based on the orientation of the O_{vac} pair within the structure. There are nine possible O_{vac} pair orientations when two O_{vacs} are introduced into the 96 atom supercell of c-ZrO_2. In order of increasing interatomic separation of the vacancy pair, these are the: ⟨1 0 0⟩, ⟨1 1 0⟩, ⟨1 1 1⟩, ⟨2 0 0⟩, ⟨2 1 0⟩, ⟨2 1 1⟩, ⟨2 2 1⟩, and ⟨2 2 2⟩ orientations. The O_{vac} pair orientation which has the fewest number of point group symmetries has the largest number of possible defect topologies; this is the ⟨1 1 0⟩ orientation. *Table 3* lists the O_{vac} pair orientations, the atomic site separation of the O_{vacs}, and the number of structures within each O_{vac} pair category.

Table 3: Crystallographic orientation, atomic site separation, and number of structures within each O_{vac} pair category in a 96 atom 2x2x2 cell of c-ZrO2.

O_{vac} pair crystallographic orientation	O_{vac} pair separation / Å	Number of structures within O_{vac} pair category
⟨1 0 0⟩	2.55	511

⟨1 1 0⟩	3.61	807
⟨1 1 1⟩	4.43	42
⟨2 0 0⟩	5.11	128
⟨2 1 0⟩	5.71	431
⟨2 1 1⟩	6.26	394
⟨2 2 0⟩	7.23	239
⟨2 2 1⟩	7.67	269
⟨2 2 2⟩	8.86	35

In *Figure 1* the total DFT energy of each relaxed configuration is plotted against the reciprocal O_{vac} site separation. Structures within the ⟨2 1 0⟩ O_{vac} pair category are predicted to be the most energetically favourable. This result is in contrast to previous theoretical studies that have suggested that the ⟨1 1 1⟩ orientation is the most favourable.[39] The energy for the lowest energy ⟨2 1 0⟩ configuration is more than 1 eV per supercell lower in energy than the lowest energy configurations in the ⟨1 1 1⟩ orientation[39]. Furthermore, the lowest energy structure found is more than 70 meV per supercell lower in energy than the next lowest energy structure. Within an energy window of 0.5 eV per supercell above the lowest energy ⟨2 1 0⟩ structure, only structures with O_{vacs} aligned along ⟨2 1 1⟩, ⟨2 1 0⟩, and ⟨1 1 0⟩ are found, with respect to all of which all ⟨1 1 1⟩ structures are found to be energetically unfavourable.

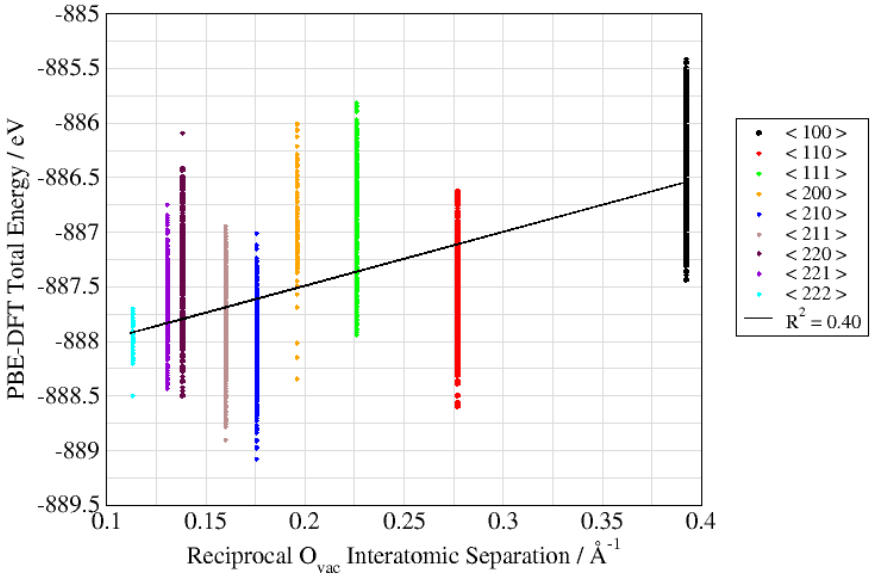

Figure 1: Total DFT energies per supercell of the relaxed configurations plotted against the reciprocal interatomic separation of the O_{vac} pair. The colours indicate the 'category' of each vacancy pair based on its crystallographic orientation.

In *Figure 2* the crystal structure of the lowest energy defect configuration is displayed. The two oxygen vacancies are indicated by small green spheres, and can be seen on the right hand side of the supercell. It is important to note that an oxygen vacancy configuration with a ⟨2 1 0⟩ orientation occurs for 36 of the 37 lowest energy defect configurations, the single exception being a low energy ⟨2 1 1⟩ configuration. Full cell relaxation of the lowest energy defect configuration results in a distortion from the cubic phase of less than 1˚.

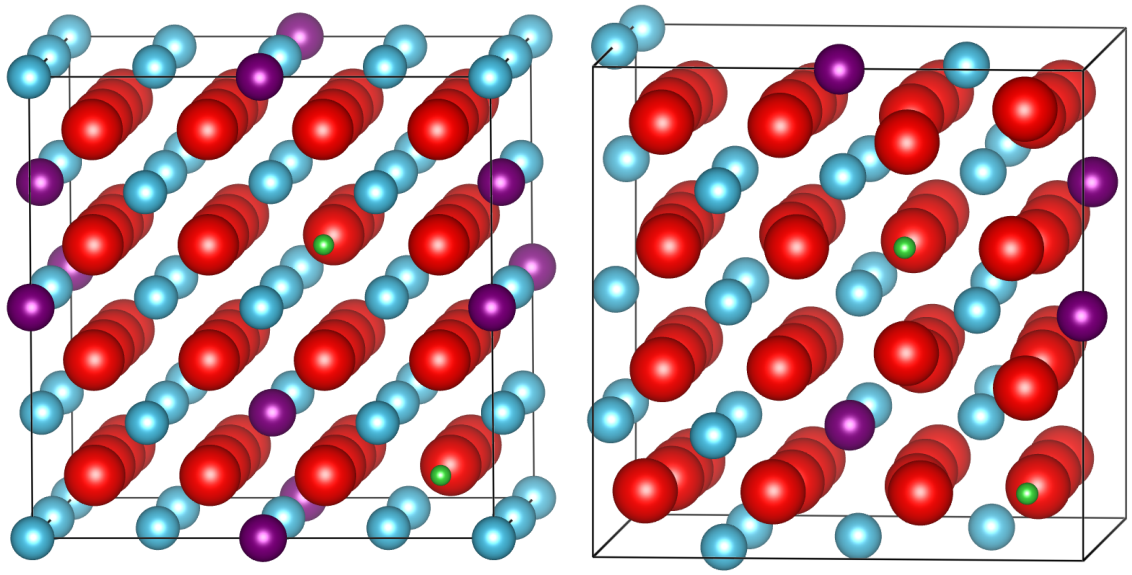

Figure 2: Crystal structure of the defect configuration predicted to have the lowest DFT energy. The O_{vac} sites (small green spheres) are oriented along the ⟨2 1 0⟩ direction. Yttrium ions in purple, zirconium ions in blue and oxygen ions in red. Left : the unrelaxed structure, right: the relaxed structure.

The trend line in *Figure 1* suggests that, in general, configurations with larger O_{vac} - O_{vac} separations possess lower energies, and by inference, there is an effective repulsive interaction between O_{vacs}. The regression (R^2) between the average energy of each vacancy pair category and the reciprocal atomic site separation of the vacancies is 0.4. This weak correlation suggests that the O_{vac} separation is not an effective descriptor of the -DFT energies. This is further highlighted by the ⟨2 1 1⟩, ⟨2 1 0⟩, and ⟨1 1 0⟩ categories whose average energies are lower than would be expected from a simple electrostatic model.

These findings provide a valuable representation of the bulk YSZ crystals at 6.7 mol%. We note that for parts of a crystal where the effects of microstructure become important, such as at grain boundaries, then the alignment of the dopant configurations may be affected.

Energy dependency on Y^{3+} ion distribution

Figure 1 reveals a wide range of energies within each O_{vac} pair orientation category with a typical variation of 1-2 eV. This variation is due to the distribution of Y^{3+} substitutions around the O_{vac} pair. A useful geometrical construction for analysing this variation is generated by considering the two O_{vacs} and four Y^{3+} of the dopants to be the vertices of a 3D shape. To analyse the distribution of Y^{3+} ions within each structure, and indeed within each vacancy pair category, we identified the lowest volume convex hull to define a characteristic polyhedron for each configuration. Possible convex hull shapes include octahedra and planar sheets. Configurations may be classified in terms of the convex hull volume, average Y^{3+} - O_{vac} interatomic separation, and average Y^{3+} - Y^{3+} interatomic separation. It is found that the total DFT energy correlates very weakly with the volume of a dopant cluster and weakly with the with the average Y^{3+} - Y^{3+} interatomic separation. There is a modest correlation between the average Y^{3+} - O_{vac} interatomic separation and the total DFT energies, implying that, in general, O_{vacs} and Y^{3+} ions have an effective attractive interaction so that it is energetically favourable for the O_{vac} to Y^{3+} ion separation to be minimised. The regression coefficient measuring this correlation for classes of configuration based on orientation is displayed in *Table 4.* This suggests that the correlation is particularly large for ⟨1 0 0⟩, ⟨1 1 0⟩, ⟨1 1 1⟩, ⟨2 0 0⟩, ⟨2 1 0⟩, and ⟨2 1 1⟩ O_{vac} orientations, with the trend being strongest in the ⟨1 1 1⟩ orientation. For the ⟨2 2 0⟩ and ⟨2 2 1⟩ orientations a

significantly weaker correlation is found and for the ⟨2 2 2⟩ there is negligible correlation. These trends are generally consistent with an ionic model of the defect interactions in which, at smaller vacancy separations, the Y^{3+} ions play the role of screening the inter-vacancy repulsion and thus tend to neighbour the O-vacancies. Indeed, in the lowest energy structure displayed in *Figure 2* the Y^{3+} ions surround the O-vacancy sites in positions that are as close as possible, subject to the constraint of maintaining 8-fold Y-O coordination, in a tetrahedral-like configuration. This effective screening interaction appears to be important for determining the stability of dopant configurations

Table 4: Regression coefficients for the correlation between Y^{3+} - O_{vac} interatomic separation and total DFT energies of the relaxed structures for each of the O_{vac} pair categories of Figure 1.

O_{vac} pair crystallographic orientation	Regression coefficient (R^2) between total DFT energies of the structures and the average Y^{3+} - O_{vac} interatomic separation.
⟨1 0 0⟩	0.53
⟨1 1 0⟩	0.58
⟨1 1 1⟩	0.65
⟨2 0 0⟩	0.57
⟨2 1 0⟩	0.49
⟨2 1 1⟩	0.50
⟨2 2 0⟩	0.31
⟨2 2 1⟩	0.33

⟨2 2 2⟩	0.01

Born-Mayer-Huggins and ReaxFF as Predictors of DFT Relaxation Energies

The internal coordinates of the 2857 symmetry inequivalent defect structures were also fully relaxed within both the BMH polarisable shell model, and ReaxFF model potentials. In *Figure 3* the relaxed DFT energies are plotted against total BMH energies for each configuration. The BMH model energies correlate poorly with the DFT energies yielding an R^2 of 0.2. The regression coefficient suggests that the correlation a 6.7mol% is significantly worse than at 3.2mol%, for which the regression coefficient has been shown to be 0.35[24]. This comparison, however, must be qualified by noting the more exhaustive DFT data set used in this work for 6.7mol%. An interesting feature shown by *Figure 3* is that the BMH model performs relatively well at predicting some of the high energy DFT structures. It is not clear whether the failure of this polarisable ion model to reproduce the DFT energies is due to its functional form or the particular parameterisation.

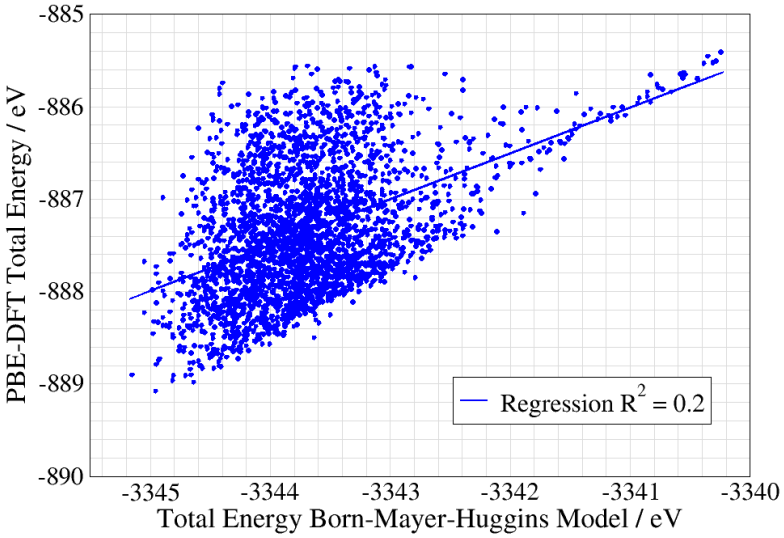

Figure 3: Born-Mayer-Huggins polarisable shell model total energies of the relaxed structures plotted against the equivalent DFT total energies of the relaxed structures.

In *Figure 4* the ReaxFF model energies are plotted against the relaxed DFT energies. The data are clustered in an elliptical distribution at the left of *Figure 4*, which suggests a weak correlation between the DFT energies and those from ReaxFF. Indeed the regression coefficient is just 0.14. On this basis, the model performs worse at predicting the relative DFT energies of the fully relaxed 6.7mol% structures than the BMH model. The ReaxFF model has a flexible functional form and so it is possible that fitting to a wider dataset of DFT energies may improve the correlation; the model used here was fitted to the relative energies of six 7.1mol% YSZ defect structures.

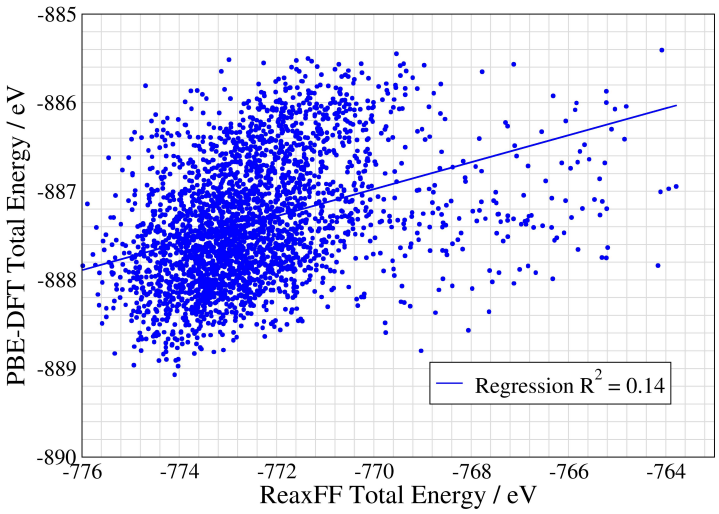

Figure 4: ReaxFF model energies of the relaxed structures plotted against the DFT total energies of the relaxed structures for the same configurations. The straight line indicates a linear least squares fit.

Coulomb Energy as a Descriptor of DFT Relaxation Energies

Although rather sophisticated models of the ionic interactions in YSZ fail to reproduce the trends in DFT energies it has been suggested that a very simple descriptor based on the electrostatic energy a point charge model, based on formal point charges calculated at the unrelaxed geometries of the configurations provides a reliable descriptor of the likely low energy long-range DFT structures at 3.2mol%. In *Figure 5* the total electrostatic energy of the unrelaxed 6.7mol% defects is plotted against the total DFT energies of the equivalent configurations. Given the complexity of the system it is perhaps surprising that the correlation between the two data sets is strong with an R^2 of 0.62.

We emphasise that the correlation of this simple descriptor with the DFT energies is not evidence that the governing interactions are predominantly electrostatic in nature. It is clear from the correlation with carefully parameterised BMH and ReaxFF potentials that these models are not capturing the variations in total energy accurately. Nevertheless, the correlation means that this quantity which can be computed efficiently for very large atomistic models can be used as the basis for a pragmatic strategy for identifying low energy structures.

If for any defect concentration one restricts defect geometries to NNN or longer range structures. Then, for each configuration the total electrostatic energies at unrelaxed geometries are computed within a formal point charge model. Retaining the *lower quartile* of energy ordered structures only and relaxing them fully in DFT calculations one would expect to capture reliably all low energy structures within 0.5 eV / 96 ions cell of the minimum energy DFT structure.

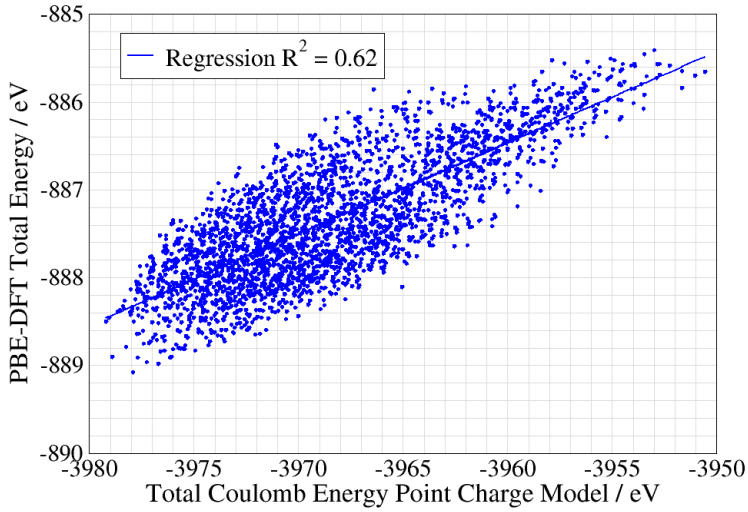

Figure 5: Total electrostatic energies per supercell of the unrelaxed structures structures plotted against the equivalent DFT total energies of the relaxed structures.

Vacancy Migrations

Having established typical low energy structures for YSZ it is interesting to re-examine the oxygen migration mechanism which underpin its use as a fast ion conductor. We consider the energetics for oxygen migration for the structure predicted to have the lowest energy by DFT (see *Figure 2*). Our goal is to understand the energy scale for the initial activation of the migration process, and in this initial study we consider only a simple single vacancy mechanism for vacancy hopping. There are two vacancies in the unit cell 94 atom supercell at 6.7mol%, and we calculate the energy for the vacancy to hop to a near-neighbour oxygen site using the nudged elastic band method on a DFT energy surface. There are six possible nearest-neighbour sites surrounding each oxygen vacancy, and in *Table 5* we present the lowest migration barrier amongst these six sites for the movement of the two vacancies. Both vacancies confront similar barriers of 0.59 and 0.57eV for their initial hops. This large barrier is consistent with those

deduced from AC impedance spectroscopy experiments[60]. We have explored subsequent hops beyond the initial barrier and find that the results vary in the range 0.1 to 0.8eV. A full analysis of these pathways is beyond the scope of the current work.

Table 5 Migration barriers for oxygen vacancy hops of the lowest DFT energy defect configuration.

Vacancy	**Lowest Barrier for Vacancy Hop (eV)**
Vacancy 1 (Green pseudo-atom shown in the centre of the structure in Fig. 2))	0.59
Vacancy 2 (Green pseudo-atom shown in the bottom right hand corner of the structure in Fig. 2) 2	0.57

Conclusion

DFT calculations have been used to document the energy of all symmetry independent dopant configurations for 6.7mol% YSZ represented in a 2x2x2 supercell of c-ZrO_2. The dopant with O-vacancies oriented along the ⟨2 1 0⟩ crystallographic direction is found to be significantly lower in energy than those in other orientations. This is in contrast to previous studies which have suggested a ⟨1 1 1⟩ orientation which is found her to be unstable by more than 1 eV per supercell. This surprising result invites a reassessment of both existing experimental and theoretical work regarding the dopant configuration in YSZ and its diffusion mechanisms.

The determination of the DFT energies for the large data set of 2857 structures has also provided a basis for the evaluation of the utility of both alternative models and structural descriptors of the DFT total energies. State of the art interatomic potential models based on the Born-Mayer-Huggins and ReaxFF forms are found to correlate poorly with the DFT energies. It is not clear if this is due to restrictions in their functional forms or details of the particular parameterisations. Other screening heuristics such as the Coulomb energy and the Y-ion separation were also explored in seeking to predict the prevalent dopant configurations. We find that while, Y^{3+} - O_{vac} separation may be useful for predicting low energy configurations for short O_{vac} separations, the calculation of the bare Coulomb interaction of an unrelaxed structure from a formal point charge model is a much more effective descriptor of low energy configurations. Based on this we suggest an efficient approach for identifying low energy dopant configurations in more complicated geometries which might include surfaces, interfaces and nanostructures.

Author Information:

Corresponding author: Michael.Parkes07@imperial.ac.uk

Acknowledgements

The authors would like to acknowledge the EPSRC for funding of this work, through a career acceleration fellowship, award number EP/I00422X/1. Images of atomic structures were prepared using Jmol[61].

References

(1) Kresse, G.; Hafner, J. Norm-Conserving and Ultrasoft Pseudopotentials for First-Row and Transition Elements. *J. Phys. Condens. Matter* **1994**, *6* (40), 8245–8257.

(2) Fergus, J. W. *Green Chemistry and Chemical Engineering Solid Oxide Fuel Cells Materials Properties and Performance*; 2009.

(3) Fergus, J. W. Electrolytes for Solid Oxide Fuel Cells. *J. Power Sources* **2006**, *162* (1), 30–40.

(4) Shishkin, M.; Ziegler, T. The Oxidation of H2 and CH4 on an Oxygen-Enriched Yttria-Stabilized Zirconia Surface: A Theoretical Study Based on Density Functional Theory. *J. Phys. Chem. C* **2008**, *112* (49), 19662–19669.

(5) Shishkin, M.; Ziegler, T. Oxidation of H2, CH4, and CO Molecules at the Interface between Nickel and Yttria-Stabilized Zirconia: A Theoretical Study Based on DFT. *J. Phys. Chem. C* **2009**, *113* (52), 21667–21678.

(6) Shishkin, M.; Ziegler, T. Hydrogen Oxidation at the Ni/Yttria-Stabilized Zirconia Interface: A Study Based on Density Functional Theory. *J. Phys. Chem. C* **2010**, *114* (25), 11209–11214.

(7) Cucinotta, C.; Bernasconi, M.; Parrinello, M. Hydrogen Oxidation Reaction at the Ni/YSZ Anode of Solid Oxide Fuel Cells from First Principles. *Phys. Rev. Lett.* **2011**, *107* (20), 206103.

(8) Ammal, S. C.; Heyden, A. Combined DFT and Microkinetic Modeling Study of Hydrogen Oxidation at the Ni/YSZ Anode of Solid Oxide Fuel Cells. *J. Phys. Chem. Lett.* **2012**, *3* (19), 2767–2772.

(9) van Duin, A. C. T.; Merinov, B. V; Jang, S. S.; Goddard, W. A. ReaxFF Reactive Force Field for Solid Oxide Fuel Cell Systems with Application to Oxygen Ion Transport in Yttria-Stabilized Zirconia. *J. Phys. Chem. A* **2008**, *112* (14), 3133–3140.

(10) Merinov, B. V.; Mueller, J. E.; van Duin, A. C. T.; An, Q.; Goddard, W. A. ReaxFF Reactive Force-Field Modeling of the Triple-Phase Boundary in a Solid Oxide Fuel Cell. *J. Phys. Chem. Lett.* **2014**, *5* (22), 4039–4043.

(11) Malavasi, L.; Fisher, C. A. J.; Islam, M. S. Oxide-Ion and Proton Conducting Electrolyte Materials for Clean Energy Applications: Structural and Mechanistic Features. *Chem. Soc. Rev.* **2010**, *39* (11), 4370–4387.

(12) Shishkin, M.; Ziegler, T. Direct Modeling of the Electrochemistry in the Three-Phase Boundary of Solid Oxide Fuel Cell Anodes by Density Functional Theory: A Critical Overview. *Phys. Chem. Chem. Phys.* **2014**, *16* (5), 1798–1808.

(13) Xia, X.; Oldman, R.; Catlow, R. Computational Modeling Study of Bulk and Surface of Yttria-Stabilized Cubic Zirconia. *Chem. Mater.* **2009**, *21* (15), 3576–3585.

(14) Badwal, S. Zirconia-Based Solid Electrolytes: Microstructure, Stability and Ionic

Conductivity. *Solid State Ionics* **1992**, *52* (1-3), 23–32.

(15) Yashima, M.; Morimoto, K.; Ishizawa, N.; Yoshimura, M. Zirconia-Ceria Solid Solution Synthesis and the Temperature-Time-Transformation Diagram for the 1:1 Composition. *J. Am. Ceram. Soc.* **1993**, *76* (7), 1745–1750.

(16) Ioffe, A. I.; Rutman, D. S.; Karpachov, S. V. On the Nature of the Conductivity Maximum in Zirconia-Based Solid Electrolytes. *Electrochim. Acta* **1978**, *23* (2), 141–142.

(17) Kharton, V. V.; Naumovich, E. N.; Vecher, A. A. Research on the Electrochemistry of Oxygen Ion Conductors in the Former Soviet Union. I. ZrO 2 -Based Ceramic Materials. *J. Solid State Electrochem.* **1999**, *3* (2), 61–81.

(18) Goff, J.; Hayes, W.; Hull, S.; Hutchings, M.; Clausen, K. Defect Structure of Yttria-Stabilized Zirconia and Its Influence on the Ionic Conductivity at Elevated Temperatures. *Phys. Rev. B* **1999**, *59* (22), 14202–14219.

(19) Bogicevic, A.; Wolverton, C.; Crosbie, G.; Stechel, E. Defect Ordering in Aliovalently Doped Cubic Zirconia from First Principles. *Phys. Rev. B* **2001**, *64* (1).

(20) Bogicevic, A.; Wolverton, C. Nature and Strength of Defect Interactions in Cubic Stabilized Zirconia. *Phys. Rev. B* **2003**, *67* (2).

(21) Parlinski, K.; Li, Z.; Kawazoe, Y. First-Principles Determination of the Soft Mode in Cubic ZrO2. *Phys. Rev. Lett.* **1997**, *78* (21), 4063–4066.

(22) Fadda, G.; Zanzotto, G.; Colombo, L. First-Principles Study of the Effect of Pressure on the Five Zirconia Polymorphs. I. Structural, Vibrational, and Thermoelastic Properties. *Phys. Rev. B* **2010**, *82* (6), 064105.

(23) Fadda, G.; Zanzotto, G.; Colombo, L. First-Principles Study of the Effect of Pressure on the Five Zirconia Polymorphs. II. Static Dielectric Properties and Raman Spectra. *Phys. Rev. B* **2010**, *82* (6), 064106.

(24) Parkes, M. A.; Refson, K.; d'Avezac, M.; Offer, G. J.; Brandon, N. P.; Harrison, N. M. Chemical Descriptors of Yttria-Stabilized Zirconia at Low Defect Concentration: An Ab Initio Study. *J. Phys. Chem. A* **2015**, *119* (24), 6412–6420.

(25) Negita, K. Lattice Vibrations and Cubic to Tetragonal Phase Transition in ZrO2. *Acta Metall.* **1989**, *37* (1), 313–317.

(26) Norberg, S. T.; Hull, S.; Ahmed, I.; Eriksson, S. G.; Marrocchelli, D.; Madden, P. A.; Li, P.; Irvine, J. T. S. Structural Disorder in Doped Zirconias, Part I: The Zr 0.8 Sc 0.2– X Y X O 1.9 ($0.0 \leq X \leq 0.2$) System. *Chem. Mater.* **2011**, *23* (6), 110223092625053.

(27) Marrocchelli, D.; Madden, P. A.; Norberg, S. T.; Hull, S. Structural Disorder in Doped

Zirconias, Part II: Vacancy Ordering Effects and the Conductivity Maximum. *Chem. Mater.* **2011**, *23* (6), 110223092559005.

(28) Li, P.; Chen, I.-W.; Penner-Hahn, J. X-Ray-Absorption Studies of Zirconia Polymorphs. II. Effect of Y2O3 Dopant on ZrO2 Structure. *Phys. Rev. B* **1993**, *48* (14), 10074–10081.

(29) Catlow, C. R. A.; Chadwick, A. V.; Greaves, G. N.; Moroney, L. M. EXAFS Study of Yttria-Stabilized Zirconia. *J. Am. Ceram. Soc.* **1986**, *69* (3), 272–277.

(30) Cole, M.; Catlow, C. R. A.; Dragun, J. P. EXAFS Studies of Doped-ZrO2 Systems. *J. Phys. Chem. Solids* **1990**, *51* (6), 507–513.

(31) Kawata, K.; Maekawa, H.; Nemoto, T.; Yamamura, T. Local Structure Analysis of YSZ by Y-89 MAS-NMR. *Solid State Ionics* **2006**, *177* (19–25), 1687–1690.

(32) Stapper, G.; Bernasconi, M.; Nicoloso, N.; Parrinello, M. Ab Initio Study of Structural and Electronic Properties of Yttria-Stabilized Cubic Zirconia. *Phys. Rev. B* **1999**, *59* (2), 797–810.

(33) Dalach, P.; Ellis, D. E.; van de Walle, A. First-Principles Thermodynamic Modeling of Atomic Ordering in Yttria-Stabilized Zirconia. *Phys. Rev. B* **2010**, *82* (14), 144117.

(34) D Steele and B E F Fender. The Structure of Cubic ZrO 2 :YO 1.5 Solid Solutions by Neutron Scattering. *J. Phys. C Solid State Phys.* **1974**, *7* (1), 1.

(35) Roth, W.; Wong, R.; Goldman, A.; Canova, E.; Kao, Y.; Dunn, B. Structure of Additives in B″ -Alumina and Zirconia Superionic Conductors. *Solid State Ionics* **1986**, *18-19*, 1115–1119.

(36) Morikawa, H.; Shimizugawa, Y.; Marumo, F.; Harasawa, T.; Ikawa, H.; Tohji, K.; Udagawa, Y. Local Structures Around Y Atoms in Y2O3-Stabilized Tetragonal ZrO2. *J. Ceram. Soc. Japan* **1988**, *96* (1111), 253–258.

(37) Tuilier, M. H.; Dexpert-Ghys, J.; Dexpert, H.; Lagarde, P. X-Ray Absorption Study of the ZrO2 Y2O3 System. *J. Solid State Chem.* **1987**, *69* (1), 153–161.

(38) Pietrucci, F.; Bernasconi, M.; Laio, A.; Parrinello, M. Vacancy-Vacancy Interaction and Oxygen Diffusion in Stabilized Cubic ZrO2 from First Principles. *Phys. Rev. B* **2008**, *78* (9), 094301.

(39) Ostanin, S.; Craven, A.; McComb, D.; Vlachos, D.; Alavi, A.; Paxton, A.; Finnis, M. Electron Energy-Loss near-Edge Shape as a Probe to Investigate the Stabilization of Yttria-Stabilized Zirconia. *Phys. Rev. B* **2002**, *65* (22), 224109.

(40) Orera, V.; Merino, R.; Chen, Y.; Cases, R.; Alonso, P. Intrinsic Electron and Hole Defects in Stabilized Zirconia Single Crystals. *Phys. Rev. B* **1990**, *42* (16), 9782–9789.

(41) Azzoni, C.; Paleari, A. Sevenfold- and Sixfold-Coordinated Zr3+ Ions in Cubic Stabilized Zirconia: Crystal-Field Approach. *Phys. Rev. B* **1991**, *44* (13), 6858–6863.

(42) Azzoni, C.; Bolis, L.; Paleari, A.; Samoggia, G.; Scardina, F. Disorder-Induced Optical and Paramagnetic Properties in Zirconium Dioxide: Role of Low-Symmetry Crystal Fields. *Phys. Rev. B* **1995**, *51* (22), 15942–15946.

(43) Azzoni, C.; Paleari, A. Photoactivation of Hole Centers in Cubic Stabilized Zirconia. *Phys. Rev. B* **1996**, *53* (1), 5–8.

(44) Pietrucci, F.; Bernasconi, M.; Di Valentin, C.; Mauri, F.; Pickard, C. EPR G-Tensor of Paramagnetic Centers in Yttria-Stabilized Zirconia from First-Principles Calculations. *Phys. Rev. B* **2006**, *73* (13), 134112.

(45) Ben-Michael, R.; Tannhauser, D.; Genossar, J. ESR Centers in Reduced Stabilized Zirconia. *Phys. Rev. B* **1991**, *43* (10), 7395–7404.

(46) Merino, R.; Orera, V.; Lomonova, E.; Batygov, S. Paramagnetic Electron Traps in Reduced Stabilized Zirconia. *Phys. Rev. B* **1995**, *52* (9), 6150–6153.

(47) Gale, J. D. GULP: A Computer Program for the Symmetry-Adapted Simulation of Solids. *J. Chem. Soc. Faraday Trans.* **1997**, *93* (4), 629–637.

(48) Parkes, M.; Refson, K.; d'Avezac, M.; Offer, G.; Brandon, N. P.; Harrison, N. Determining Surface Chemistry and Vibrational Properties of SOFC Anode Materials Through Ab Initio Calculations. *ECS Trans.* **2013**, *57* (1), 2419–2427.

(49) Kresse, G. Efficient Iterative Schemes for Ab Initio Total-Energy Calculations Using a Plane-Wave Basis Set. *Phys. Rev. B* **1996**, *54* (16), 11169–11186.

(50) Perdew, J. P.; Burke, K.; Ernzerhof, M. Generalized Gradient Approximation Made Simple. *Phys. Rev. Lett.* **1996**, *77* (18), 3865–3868.

(51) Kresse, G.; Joubert, D. From Ultrasoft Pseudopotentials to the Projector Augmented-Wave Method. *Phys. Rev. B* **1999**, *59* (3), 1758–1775.

(52) Monkhorst, H. J.; Pack, J. D. Special Points for Brillouin-Zone Integrations. *Phys. Rev. B* **1976**, *13* (12), 5188–5192.

(53) Balducci, G.; Kašpar, J.; Fornasiero, P.; Graziani, M.; Islam, M. S.; Gale, J. D. Computer Simulation Studies of Bulk Reduction and Oxygen Migration in CeO 2 –ZrO 2 Solid Solutions. *J. Phys. Chem. B* **1997**, *101* (10), 1750–1753.

(54) Balducci, G.; Kašpar, J.; Fornasiero, P.; Graziani, M.; Islam, M. S. Surface and Reduction Energetics of the CeO 2 –ZrO 2 Catalysts. *J. Phys. Chem. B* **1998**, *102* (3), 557–561.

(55) Khan, M. S.; Islam, M. S.; Bates, D. R. Cation Doping and Oxygen Diffusion in Zirconia: A Combined Atomistic Simulation and Molecular Dynamics Study. *J. Mater. Chem.* **1998**, *8* (10), 2299–2307.

(56) Dwivedi, A.; Cormack, A. N. A Computer Simulation Study of the Defect Structure of Calcia-Stabilized Zirconia. *Philos. Mag. A* **1990**, *61* (1), 1–22.

(57) Lewis, G. V; Catlow, C. R. A. Potential Models for Ionic Oxides. *J. Phys. C Solid State Phys.* **1985**, *18* (6), 1149–1161.

(58) van Duin, A. C. T.; Merinov, B. V; Han, S. S.; Dorso, C. O.; Goddard, W. A. ReaxFF Reactive Force Field for the Y-Doped BaZrO3 Proton Conductor with Applications to Diffusion Rates for Multigranular Systems. *J. Phys. Chem. A* **2008**, *112* (45), 11414–11422.

(59) Lahiri, J.; Mayernick, A.; Morrow, S. L.; Koel, B. E.; van Duin, A. C. T.; Janik, M. J.; Batzill, M. Modification of Active Sites on YSZ(111) by Yttria Segregation. *J. Phys. Chem. C* **2010**, *114* (13), 5990–5996.

(60) Gibson, I. R.; Irvine, J. T. S. Study of the Order?disorder Transition in Yttria-Stabilised Zirconia by Neutron Diffraction. *J. Mater. Chem.* **1996**, *6* (5), 895.

(61) Jmol: an open-source Java viewer for chemical structures in 3D. http://www.jmol.org/ (accessed Aug 19, 2014).